

## Supporting Information

# Planar Defect Driven Growth Mechanism of Oxygen Deficient Tungsten Oxide Nanowires

Adam M. Smith<sup>1</sup>, Matthew G. Kast<sup>1,2</sup>, Benjamin A. Nail<sup>1</sup>, Shaul Aloni<sup>3</sup>, Shannon W. Boettcher<sup>1,2</sup>

1. Department of Chemistry, University of Oregon, Eugene, Oregon 97403, United States  
2. Center for Sustainable Materials Chemistry, University of Oregon, Eugene, Oregon 97403, United States  
3. Molecular Foundry, Lawrence Berkeley National Laboratory, Berkeley, California, United States

### Supporting Experimental:

**Reactor Design and NW Synthesis.** The reactor assembly consists of a multi-zone tube furnace controlled by a custom-built Omega PID apparatus, enabling LabView-based temperature control.

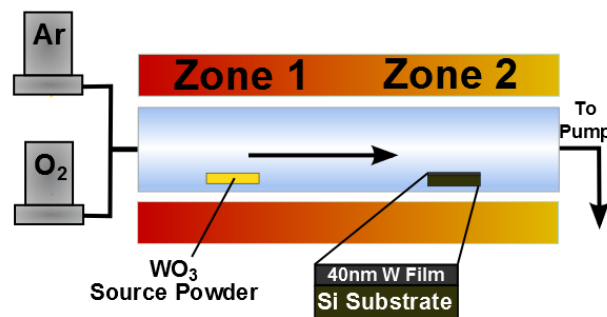


**Figure S1.** Reactor schematic illustrating two-zone geometry.

During growth runs, the substrate heating is begun and allowed to reach 200 °C before initiating the source zone heating. This constrains  $T_{\text{Substrate}} > T_{\text{Source}}$  for the duration of the ramp-up phase and inhibits material deposition below target reaction temperatures. Similarly, the source zone is closer to the exterior of the furnace, resulting in a slightly faster cooling rate. This geometry prevents deposition from the source to substrate during cooling.

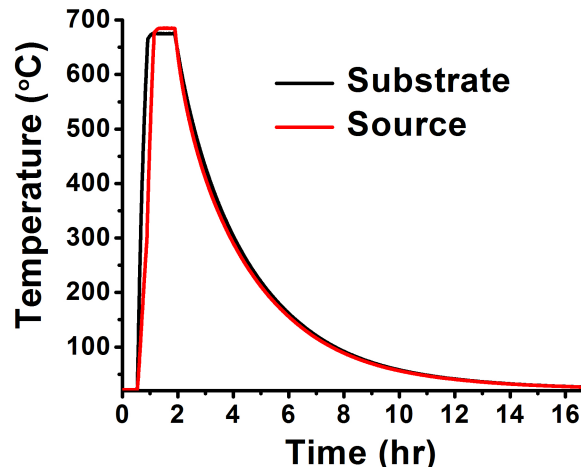


**Figure S2.** Experimentally measured NW growth temperature profile with source and substrate temperatures in red and black respectively. Notice that the source is only hotter than the substrate during the limited growth window.

**Focused Ion Beam (FIB) Milling.** NW cross-sections were prepared by FIB milling. NWs were first transferred to a Si wafer with a thermal oxide by sliding the sample linearly across the Si. A ~50 nm carbon contrast layer was deposited by thermal evaporation. Following C deposition, samples were mounted and thin bead of Pt deposited using the electron gun over the region of interest (Fig. S3A). A second Pt protecting layer was then deposited using the ion gun (Fig. S3B). The area around the region of interest was milled (Fig. S3C) and subsequently thinned using the contrast between the two different Pt films to indicate the region of interest. Thinning was performed at decreasing accelerating voltages until the sample became electron transparent (Fig. S3D and insert) to prevent beam damage and re-deposition of ablated materials. After mounting on a silicon half-TEM grid (Dune Sciences, Eugene, OR), NW samples were stored under vacuum until TEM imaging.

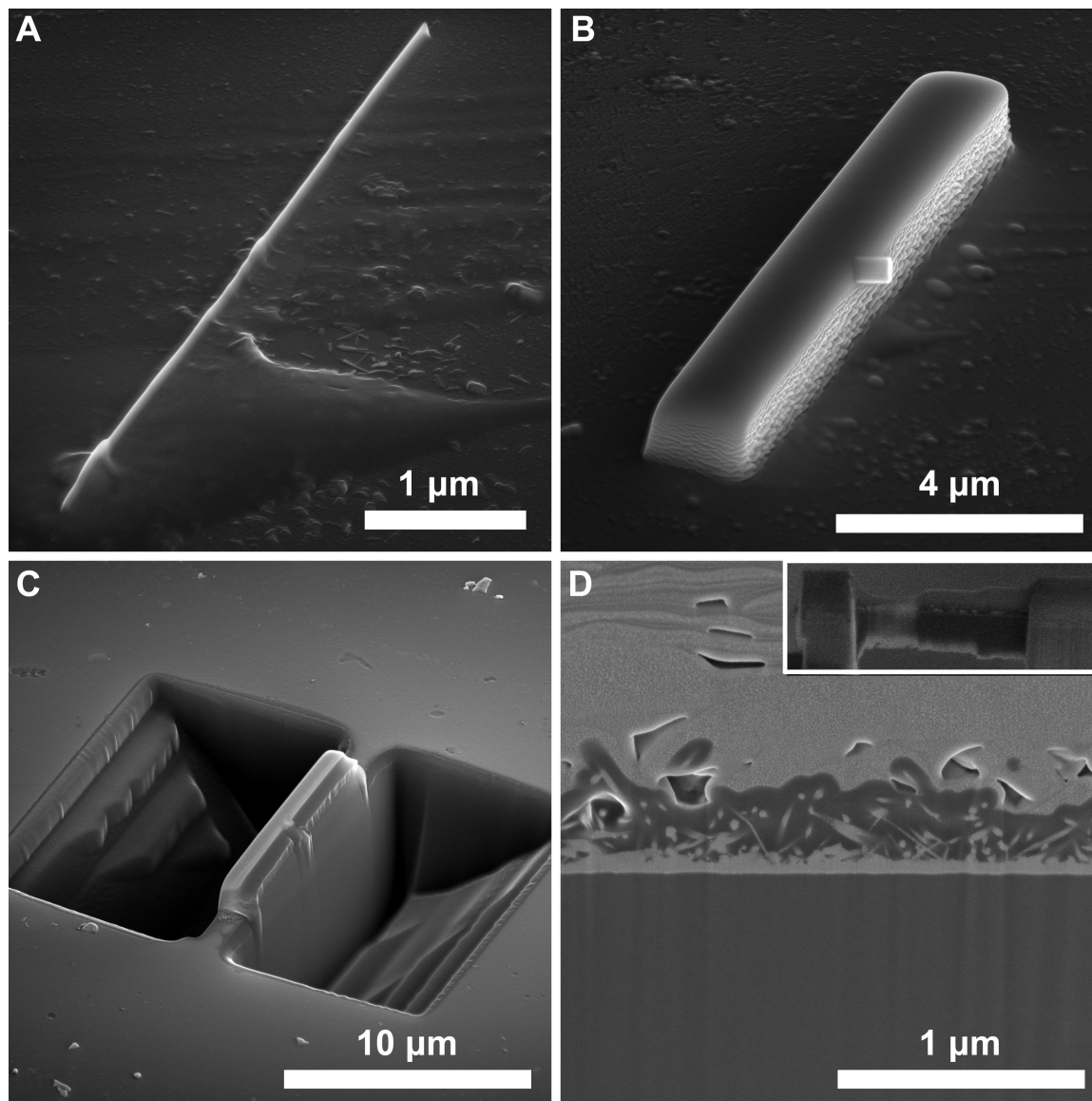


**Figure S3.** SEM images of the steps in the preparation of a representative cross-sectional NW sample. (A) Deposition of Pt bead over region of interest using the electron beam (previously coated with a blanket layer of C). (B) Larger Pt protecting layer deposited using the ion-beam. (C) Ion milling of sample. (D) Sample thinning showing presence of NWs in cross section and partially electron transparent sample (inset).

#### Supporting Characterization:

**Characterization of Growth Substrates.** The thickness of W growth substrates was measured using X-ray reflectivity (XRR) on a Bruker AKS D8 Discover diffractometer. Reflectivity measurements were acquired at three spots on the sputtered W films and modeled using Bede Refs (Bede Scientific, UK).

For some experiments, tungsten oxide growth substrates were used instead of W. To ensure the  $\text{WO}_3$  substrate was fully oxidized from the initial W film, the stoichiometry was measured after air annealing using XPS analysis. Figure S4 shows that the spectra can be fitting well without introducing a  $\text{W}^{5+}$  component, indicating a fully oxidized growth substrate.

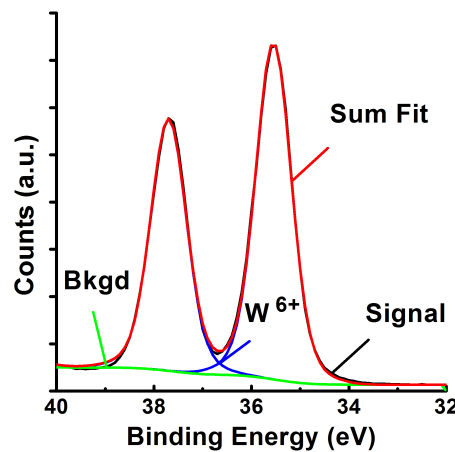


**Figure S4.** XPS analysis of  $\text{WO}_3$  growth substrate.

**Characterization of Nanostructured Films.** XRD analysis of the films was performed on a Scintag XDS 2000 diffractometer with an Inel CPS 120 linear detector and a 16 hr collection time. The XRD patterns were background subtracted and smoothed in Inel Peakoc software. Figure S5 illustrates the similarity of the XRD patterns even from films with different stoichiometry.

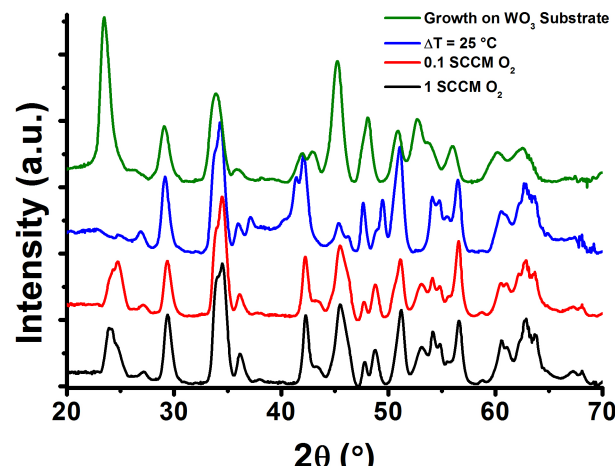


**Figure S5.** XRD analysis of nanostructured tungsten oxide films. Samples characterized include films grown with 1 SCCM  $\text{O}_2$  (black), with 0.1 SCCM  $\text{O}_2$  (red), under larger supersaturation with  $T_{\text{Source}} - T_{\text{Sub}} = 25^\circ\text{C}$  (blue), and on  $\text{WO}_3$  substrate (green).

**X-ray Photoelectron Spectroscopy (XPS) and Calculation of Substoichiometry.** XPS was performed on an ESCALAB 250 (ThermoScientific) with a monochromatic Al X-ray source set at 150 W with a 500  $\mu\text{m}$  spot size. The W4f and Au4f regions were scanned 15 times with a pass energy of 20 eV. Data analysis was performed using ThermoScientific Avantage v4.75 software. A “Smart” fit was employed to subtract the backgrounds of all spectra. Approximately 1 nm of Au was thermally evaporated on all the samples and all binding energies were calibrated by setting the Au4f<sub>7/2</sub> peak to 84.0 eV. Two peaks were used to fit the W4f<sub>7/2</sub> and W4f<sub>5/2</sub> peaks for each tungsten environment. During peak fitting the following constraints were set; the binding energy of the W4f<sub>5/2</sub> peak for a given environment was set to  $2.18 \pm 0.1$  eV higher than that of the W4f<sub>7/2</sub>, the height of the W4f<sub>5/2</sub> was set to 75% of the height of the W4f<sub>7/2</sub> peak, the FWHM of all W4f peaks for a given sample were constrained to be equal, the Lorentzian-Gaussian % (LG) was constrained to be equal for all W peaks for a given sample. An unconstrained W5p<sub>3/2</sub> peak was included in the fit (location, height and FWHW unconstrained, LG constrained as mentioned before) at  $\sim 41.5$  eV as this peak overlaps with the W4f peaks at higher binding energies.

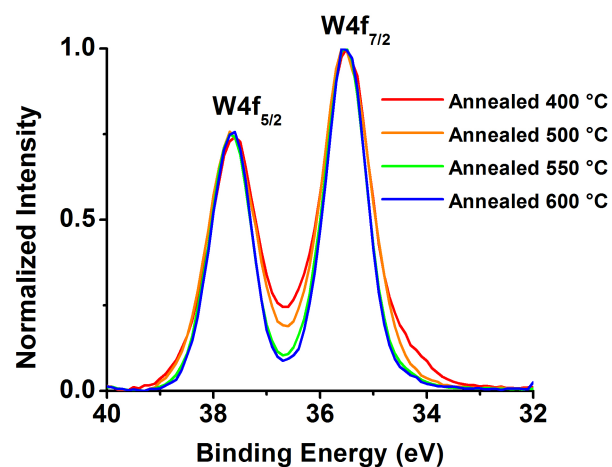


**Figure S6.** Normalized and background subtracted experimental XPS spectra of oxidized NW samples.

The ratio of the areas of the W4f<sub>7/2</sub> peaks assigned to the W<sup>+6</sup> and W<sup>+5</sup> (lower binding energy) was used to determine the ratio of W<sup>+6</sup> to W<sup>+5</sup> in the samples. We note that the  $\sim 1.4$  eV shift to lower binding energies is consistent with the expected shift between W<sup>+6</sup> and W<sup>+5</sup> and is too small to be a shift between W<sup>+6</sup> and W<sup>+4</sup> species.<sup>1, 2</sup> To test for the presence of W<sup>+4</sup> species an additional set of peaks for the W<sup>+4</sup> environment were used, which always resulted in poorer fits or the W<sup>+4</sup> peak heights converging to zero. To calculate the O to W ratio ( $R_{\text{O/W}}$ ) and subsequent stoichiometry an average environment of 3 O atoms for each W<sup>+6</sup> and 2.5 O for W<sup>+5</sup> was assumed.<sup>3</sup> The atomic % of the W4f peaks were used in equation 1:

$$R_{O/W} = \frac{(3 \cdot W^{6+} + 2.5 \cdot W^{5+})}{(W^{6+} + W^{5+})} \quad (1)$$

In order to measure the error in the W:O ratios, the standard deviation of three spots on each sample was used (e.g.  $\pm 0.01$ ). Additionally, normalized intensities of the experimental XPS spectra are compared in Figure S6. The additional signal in the valley between the  $W4f_{7/2}$  and  $W4f_{5/2}$  peaks and in the shoulders are indicative of  $W^{+5}$  species and illustrates the ability to experimentally differentiate between more and less oxidized samples, even at small differences in stoichiometry. For the NW samples annealed at 550 °C and 600 °C, the  $W^{+5}$  features are less pronounced, making a significant distinction between stoichiometry difficult.

**SEM imaging of NW film annealed at 600 °C.** After annealing in air for 30 min at 600 °C, the film was cleaved and imaged in both cross sectional and planar geometries. Figure S6 illustrates the complete collapse of 1-D structure after annealing as well as the delamination (Fig. S6.B) of the film from the substrate.

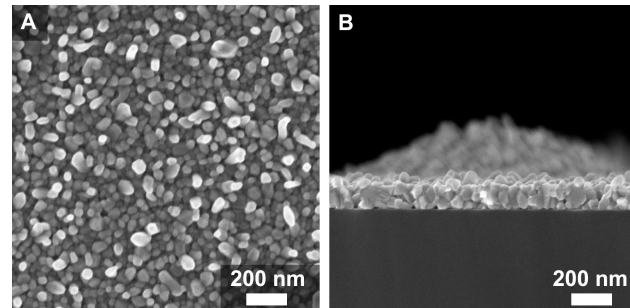


**Figure S7.** SEM images of the NW films annealed at 600 °C. (A) Planar and (B) cross-sectional images showing collapse of the 1D nanostructure.

### Supporting References:

1. K. Senthil and K. Yong, *Nanotechnology*, 2007, **18**.
2. A. Temmink, O. Anderson, K. Bange, H. Hantsche and X. Yu, *Thin Solid Films*, 1990, **192**, 211-218.
3. E. S. W.-D. Lassner, *Tungsten : Properties, Chemistry, Technology of the Element, Alloys, and Chemical Compounds*, Kluwer Academic/Plenum Publishers, New York, 1999.